A Comparison of Outer Rotor Radial and Axial Flux Machines for Application in Electric Vehicles

Vandana Rallabandi[1], Oluwaseun A. Badewa[2], Burak Ozpineci[1] and Dan M. Ionel[2]
[1]National Transportation Research Center, Oak ridge national laboratory, Knoxville, USA
[2]SPARK Laboratory, ECE Department, University of Kentucky, Lexington, KY, USA
rallabandivp@ornl.gov, o.badewa@uky.edu, burak@ornl.gov and dan.ionel@ieee.org

***Abstract*—Axial flux machines have attracted a lot of interest in the recent years as potential high torque low weight candidates for use as traction motors in electric vehicles (EV). This paper compares axial and radial flux machines for electric vehicle applications. An external rotor radial flux machine with a Halbach array surface permanent magnet rotor and concentrated windings is chosen as a baseline to compare with axial flux designs. Both axial and radial flux motors are sized to meet the EV same requirements. Multi-objective design optimization using differential evolution minimizing loss and volume is carried out for both types of machines. Hundreds of candidate designs for each type of machine are analyzed, pareto fronts are identified and compared. The potential advantages of axial flux machines are evaluated and quantified.**

***Index Terms*—Permanent magnet machine, axial flux motors**

I. Introduction

Axial flux motors have attracted a significant amount of interest in recent years [1-5]. . Although several original equipment manufacturers make claims of high torque density and a small amount of work comparing the two types of machines has been reported in the literature [6-8], these comparisons have been conducted for single, non-optimized designs of each type of machine. Many of these comparisons also rely on analytical formulations and approximations, which may not be applicable to an axial flux machine which requires 3D field solutions to obtain an accurate estimate of performance. Thus, a systematic comparison between the two machine topologies is missing.

Outer rotor radial flux machines are gaining interest because of the ability to have a higher airgap diameter for the same overall diameter as well as no requirement of magnet retention in the airgap. Thus, such machines have a potential for high power density [9] . Similarly, the two-rotor segmented stator axial flux motor, YASA is also a candidate for high power density due to the elimination of the rotor yoke [10].

This work reports on a systematic comparison between radial and axial flux permanent magnet motors. Two high power density machine candidates are compared: An outer rotor surface permanent magnet rotor, and a 2-rotor YASA type axial flux motor. Both types of machines are sized and optimized for passenger EV applications, and optimized versions of the machines are compared.

This manuscript has been authored by UT-Battelle LLC under contract DE-AC05-00OR22725 with the US Department of Energy (DOE). The US government retains and the publisher, by accepting the article for publication, acknowledges that the US government retains a nonexclusive, paid-up, irrevocable, worldwide license to publish or reproduce the published form of this manuscript, or allow others to do so, for US government purposes. DOE will provide public access to these results of federally sponsored research in accordance with the DOE Public Access Plan (http://energy.gov/downloads/doe-public-access-plan)

II. Radial flux motor design

This study focuses on motors for light duty passenger vehicles rated for 50kW continuous power, operating at a speed of 6500rpm. The radial flux PMSM (RFPM) design with fractional slot concentrated winding and 18 stator slots and 16 rotor poles for this application is based on the design reported by the authors in [9]. The motor features an outer rotor with Halbach array permanent magnets, with 2-magnet segments per pole (Fig. 1). A parametric model including design variables (TableI) is created. In addition to the airgap, 5-dimensional ratios are used to represent different geometric parameters including the magnet radial thickness, rotor yoke thickness, coil depth, coil width and stator yoke thickness. The definitions of these ratios are below:

$$kMagnetThickness = \frac{MagnetID}{MagnetOD}$$

$$kRotorYokeThickness = \frac{MagnetOD}{RotorOD},$$

$$kCoilDepth = \frac{2 * CoilDepth}{StatorOD}$$

$$kCoilWidth = \frac{2 * CoilWidth}{StatorOD * sin(\frac{\theta_{sp}}{2})}$$

$$kStatorYokeThickness = \frac{StatorID}{2 * (StatorOD/2 - CoilDepth)}$$

Two -dimensional transient finite element analysis is employed, and almost 900-candidate RFPM designs are analyzed. The slot fill factor, current density and stator outer diameter is maintained the same in all the designs. All designs produce the same torque and this is ensured by modifying the stack length from design to design. Demagnetization is taken into account by constraining the flux density in the permanent magnets.

The objectives are to minimize the active machine volume as well as loss. Differential evolution is employed. The machine active volume is calculated as: $\frac{\pi}{4}(OD^2 - ID^2)L_{ax}$, where OD and ID are the overall machine diameters including the end

Parameter	Minimum	Maximum
Airgap[mm]	1	2
kMagnetThickness	0.8	0.9
kRotorYokeThickness	0.95	0.98
kCoilDepth	0.2	0.4
kCoilWidth	0.2	0.4
kStatorYokeThickness	0.7	0.9

Table I: Design parameters for the RFPM machine and their ranges

winding, and L_{ax} is the machine axial length including the end winding (Fig. 2).

The variation of loss with active volume for all the analyzed designs along with the pareto front is shown in Fig. 3. Three designs are selected: minimum loss, minimum volume and a design achieving the best trade-off between volume and loss and shown in Fig. 4. The values of the design variables for the selected designs are shown in TableII. The minimum volume design (Fig.4a) achieves its objective by increase in the stator slot area, which allows for a higher number of ampere turns and therefore higher electric loading, thereby increasing torque per unit volume. Likewise, in case of the minimum loss design (Fig.4c), the optimization algorithm increases the magnet height and minimizes slot area. It is seen that the some of the design parameters are pushed to the limits for the minimum loss design. This indicates that lower loss designs may be found if the constraints on these parameters are relaxed.

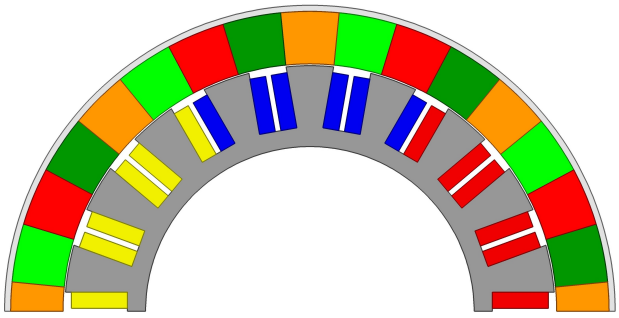

Figure 1: Cross section of the radial flux PM machine used as a baseline.

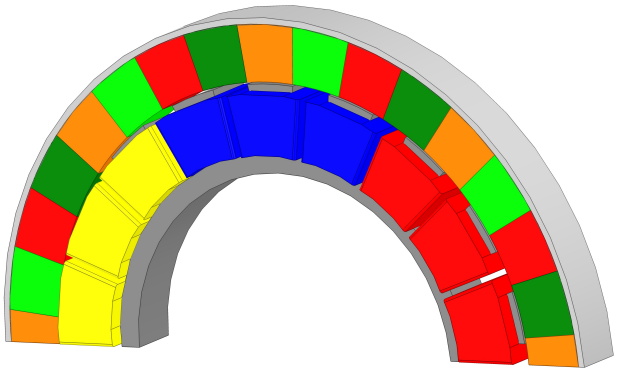

Figure 2: Three-dimensional drawing of the radial flux machine illustrating the envelope used for volume calculations.

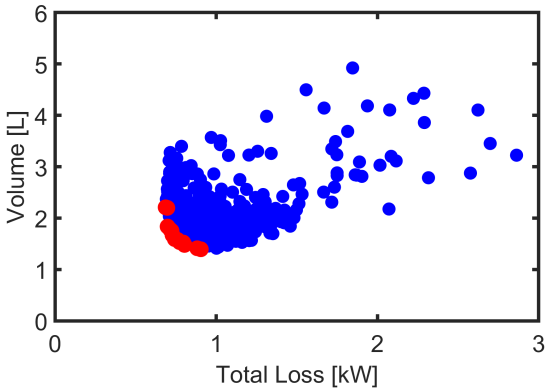

Figure 3: Loss versus active volume for all the analyzed RFPM designs.

Parameter	Min. volume	Best trade-off	Min. loss
Airgap	0.058	0	0.17
kMagnetThickness	0.24	0.15	0
kRotorYokeThickness	0.96	0.96	1
kCoilDepth	0.46	0.14	0
kCoilWidth	0.75	0.76	0.23
kStatorYokeThickness	0.9	0.5	0.22

Table II: Design parameters for the selected RFPM designs in per unit. A value of 0 means that the design parameter is set to the lower limit of the range, likewise, a value of 1 indicates that the design parameter is set to its maximum value.

The comparison of the optimized radial and axial flux machine designs is summarized (Table V). Both machines provide the same torque, and are designed with the same slot area and the same area is allocated for the windings.

III. Axial Flux Machine Design

A 2-rotor single central yokeless segmented stator construction axial flux configuration is considered, originally proposed in [11]. The machine is sized for the same 50kW continuous power as the RFPM, and employs the same slot-pole combination of 18/16. Similar to the RFPM, a two-objective differential evolution based optimization algorithm is employed to minimize both loss and active volume. Three-dimensional time-stepped FEA is employed for the design evaluations and almost 600 candidate designs are analyzed. Parametric models are developed and the parameters include current density, airgap, total axial length and 5-non-dimensional geometric ratios (TableIII). The non-dimensional ratios are defined as below:

$$RatioRotorYoke = \frac{RotorYokeThickness}{AxialLength}$$

$$RatioMagnetThickness = \frac{MagnetThickness}{AxialLength},$$

$$SplitRatio = \frac{StatorID}{StatorOD}$$

$$RatioOverHangOD = \frac{RotorOD - StatorOD}{2 * CoilThickness}$$

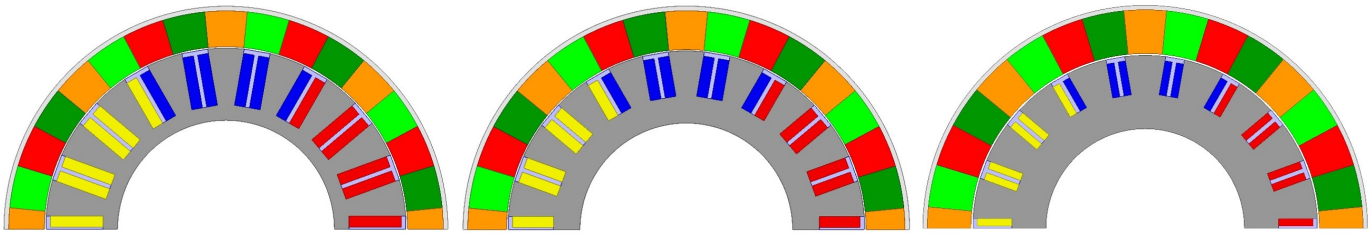

(a) (b) (c)

Figure 4: Selected RFPM designs on the Pareto front: (a) Minimum volume, (b) Best-trade off design and (c) Minimum loss

Parameter	Minimum	Maximum
Airgap[mm]	1	2
RatioRotorYoke	0.1	0.16
RatioMagnetThickness	0.1	0.25
SplitRatio	0.4	0.8
RatioOverHangOD	-1	1
RatioSlotWidthID	0.58	0.88
TotalAxialLength[mm]	40	100

Table III: Design parameters for the AFPM machine and their ranges

$$RatioSlotWidthID = \frac{SlotWidth}{SlotPitchAtID}$$

The stator outer diameter and slot fill factor are maintained the same for all designs. The current density is adjusted in each design in order to ensure that all the candidate designs produce the same torque. The 3D model of the AFPM used in the studies is shown (Fig. 5) . The loss versus active volume for all designs is shown (Fig.6). Three Pareto front designs - minimum volume, minimum loss, and the design with the best trade-off between loss and volume are shown (Fig.7). The values of the design parameters for the three selected AFPM designs are shown in Table IV. It is seen that some values are pushed to the limits for the minimum volume design, indicating that a lower volume design may be found if the limits of the optimization are expanded. The optimization algorithm reduces the split ratio, increases magnet height in order to minimize loss and pushes the current density close to its lower limit. In case of the least volume design, the split ratio is close to its maximum limit and current density is increased to obtain the target torque.

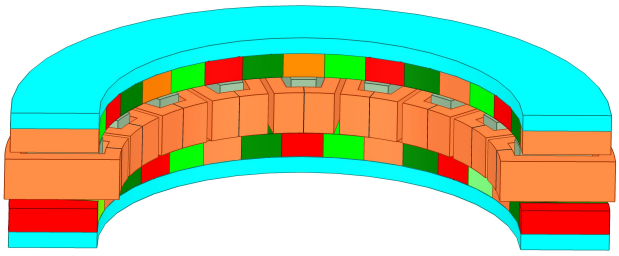

Figure 5: Parametric model of the AFPM motor used in the optimization study

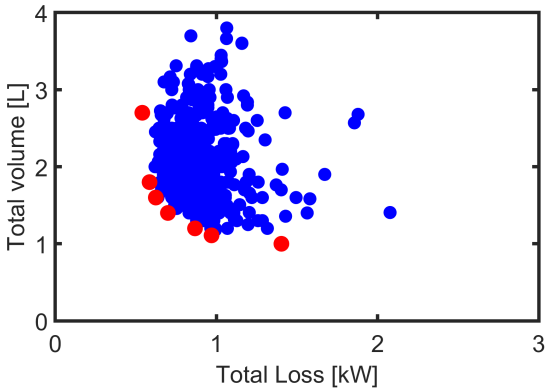

Figure 6: Loss versus active volume for all the analyzed AFPM designs.

Parameter	Min. volume	Best trade-off	Min. loss
Jratio	0.89	0.17	0.033
Airgap	0.51	0.50	0.27
RatioRotorYoke	0.024	0.0023	0.09
RatioMagnetThickness	0	0.39	0.89
SplitRatio	1	0.78	0.25
RatioOverHangOD	1	0.78	0.25
RatioSlotWidthID	0.37	0.43	0.93
TotalAxialLength	0.017	0.13	0.53

Table IV: Values of the design parameters for the optimized AFPM designs in per unit. 0 is the lower limit of the range, and 1 the higher limit.

IV. Results and Discussion

The Pareto fronts for the axial and radial flux motors are shown in Fig.8. It may be observed that over the considered design space, the AFPM designs have lower active volume than their radial flux counterparts. The best trade-off AFPM and RFPM machines are compared (TableV). It may be observed in this study that both machines produce approximately the same torque within a specified envelope. However, the axial flux machine has a somewhat lower active mass than the RFPM.

The variation of active mass with loss for all the analyzed designs of both machine types is shown in Fig. 9. Although many designs of the AFPM and RFPM have comparable weights and loss, lower weight AFPM designs which have the same loss can be found. Thus, it appears that low weight

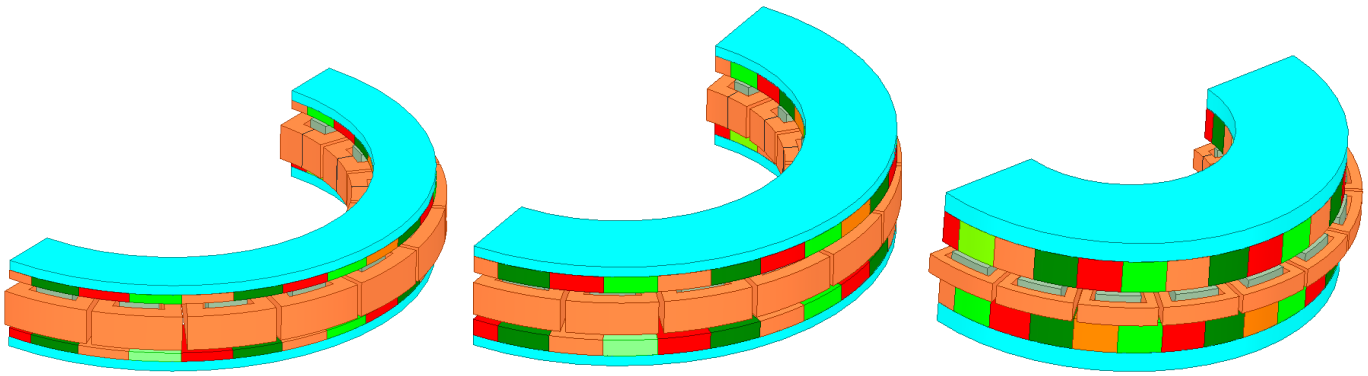

(a) (b) (c)

Figure 7: Selected AFPM designs on the Pareto front: (a) Minimum volume, (b) Best-trade off design and (c) Minimum loss

applications may favor AFPM machines. It may be noted that these observations are based on active material weight estimates, and mechanical design and inclusion of inactive components may modify these results.

Other aspects include thermal and mechanical design. It is expected that outer rotor radial flux machines may present some cooling challenges due to the location of the winding in the inner stator with lower surface area available for cooling. In cases where high operating speeds are required, permanent magnet retention would be needed for both machines. In this regard, both outer rotor radial flux machine and axial flux machines would have advantages over the traditional widely used inner rotor machines, in that magnet retention would not increase the electromagnetic airgap.

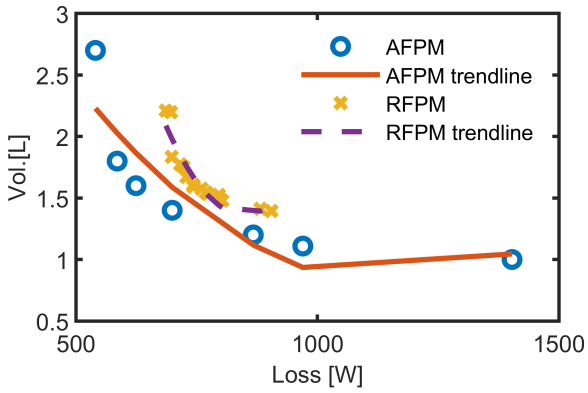

Figure 8: Loss-volume Pareto fronts for the RFPM and AFPM designs. All designs produce the same torque

V. Conclusion

This paper compares radial and axial flux machines designed for light duty electric vehicle applications. The comparison is conducted for optimized radial and axial flux machines, over a design space constituting hundreds of candidate designs in each case. The performance of each design is calculated from 2D and 3D finite element analysis. Differential evolution

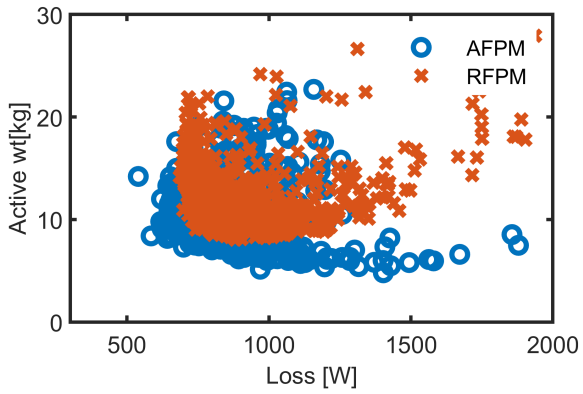

Figure 9: Loss versus mass for all the analyzed AFPM and RFPM designs

	RFPM	AFPM
Overall diameter[mm]	242	238
Inner diameter[mm]	115	140
Axial length [mm]	44	48
Torque [Nm]	75	75
Active weight [kg]	9.3	7.3
Active volume [L]	1.6	1.4
Total cylindrical volume [L]	2	2.12
Current density $[A/mm^2]$	12	11.4
Stator loss [kW]	0.759	0.699

Table V: Comparison of the best trade-off RFPM and AFPM designs.

is employed to minimize both loss and volume. It is found that over the considered design space, for a given outer diameter, both axial and radial flux would need the same axial length to provide a target torque. The analysis indicates that the axial flux machines tend to have a slightly lower active volume than the radial flux designs. The loss in both types of machines is also comparable. The results based on active weight estimates also indicate when both types of machines are designed to provide the same torque, axial flux machines may offer a weight advantage. However, mechanical design and consideration of inactive components may affect the results. Ultimately, the choice of machine topology would also need to

be governed by other aspects such as thermal considerations, or ease of integration with the vehicle.

REFERENCES

[1] F. Nishanth, J. V. Verdeghem and E. L. Severson, "Recent Advances in Analysis and Design of Axial Flux Permanent Magnet Electric Machines," 2021 IEEE Energy Conversion Congress and Exposition (ECCE), Vancouver, BC, Canada, 2021, pp. 3745-3752.

[2] N. Blanken, M. Bieber and B. Ponick, "Design of Axial End Region of Additively Manufactured Rotors of Synchronous Machines to Reduce the Axial Magnetic Stator Flux Density," 2022 International Conference on Electrical Machines (ICEM), Valencia, Spain, 2022, pp. 1505-1510.

[3] A. Allca-Pekarovic, P. J. Kollmeyer, A. Forsyth and A. Emadi, "Experimental Characterization and Modeling of a YASA P400 Axial Flux PM Traction Machine for Electric Vehicles," 2022 IEEE Transportation Electrification Conference & Expo (ITEC), Anaheim, CA, USA, 2022, pp. 433-438

[4] D. J. Patterson, G. Heins, M. Turner, B. J. Kennedy, M. D. Smith and R. Rohoza, "An overview of the compactness of a range of axial flux PM machines," 2017 IEEE Workshop on Electrical Machines Design, Control and Diagnosis (WEMDCD), Nottingham, UK, 2017, pp. 27-32.

[5] Taran, N., Rallabandi, V., Heins, G., and Ionel, D. M., "Systematically Exploring the Effects of Pole Count on the Performance and Cost Limits of Ultra-High Efficiency Fractional hp Axial Flux PM Machines," IEEE Transactions on Industry Applications, Vol. 56, No. 1, pp. 117-127 (2020)

[6] D. J. Patterson, J. L. Colton, B. Mularcik, B. J. Kennedy, S. Camilleri and R. Rohoza, "A comparison of radial and axial flux structures in electrical machines," *IEEE International Electric Machines and Drives Conference*, Miami, FL, USA, 2009, pp. 1029-1035.

[7] A. A. Pop, M. Radulescu, H. Balan and H. Kanchev, "Electromagnetic torque capabilities of axial-flux and radial-flux permanent-magnet machines," 2013 4th International Symposium on Electrical and Electronics Engineering (ISEEE), Galati, Romania, 2013, pp. 1-4.

[8] Chai, Y. Bi and L. Chen, "A Comparison between Axial and Radial Flux Permanent Magnet In-Wheel Motors for Electric Vehicle," *International Conference on Electrical Machines (ICEM)*, Gothenburg, Sweden, 2020, pp. 1685-1690

[9] T. Raminosoa et al., "A High-Speed High-Power-Density Non-Heavy Rare-Earth Permanent Magnet Traction Motor," *IEEE Energy Conversion Congress and Exposition*, 2020, pp. 61-67.

[10] T. J. Woolmer and M. D. McCulloch, "Analysis of the Yokeless And Segmented Armature Machine," 2007 IEEE International Electric Machines & Drives Conference, Antalya, Turkey, 2007, pp. 704-708.

[11] D. Talebi, M. C. Gardner, S. V. Sankarraman, A. Daniar and H. A. Toliyat, "Electromagnetic Design Characterization of a Dual Rotor Axial Flux Motor for Electric Aircraft," *IEEE International Electric Machines & Drives Conference (IEMDC)*, 2021, pp. 1-8